Short-term variability of phytoplankton blooms associated with a cold eddy in the northwestern Arabian Sea

DanLing Tang*, Hiroshi Kawamura, Alvarinho J. Luis

Center for Atmospheric and Oceanic Studies, Graduate School of Science, Tohoku University, Sendai 980-8578, Japan

Abstract

The northern Arabian Sea is a semienclosed sea with high primary productivity and a complicated flow pattern consisting of several eddies. This paper reports on phytoplankton blooms, which were associated with a cold eddy in the northern Arabian Sea during November 1996, inferred from Ocean Color and Temperature Scanner (OCTS) and Sea-view Wide Field-of-view Sensor (SeaWiFS)-derived chlorophyll *a* (Chl-a hereafter), AVHRR sea surface temperature (SST), and other available oceanography data. The blooms emerged at 100 km from both coasts in the Gulf of Oman (60.5°E, 24.5°N) where the depth is about 3000 m. The Chl-a concentrations patch first appeared on November 2 and decayed after about 4 weeks (December 3, 1996). The high Chl-a concentrations patch was about 100 km in diameter and it was located at 60.3–61.3°E, 23.5–24.5°N. The bloom, having a mean Chl-a concentration of 6.8 mg m^{-3} on November 6, was located in a cold SST eddy, which was accompanied by another feature, an anticyclone eddy (of 100 km in diameter) with high SST and low Chl-a concentrations to the southwest (61.5°E, 22.5°N). An SST drop occurred around November 14, which coincides with a peak of the vertical pumping velocity derived from NSCAT-derived wind stress. Two SeaWiFS-derived Chl-a images obtained in November 1998 and 1999 show good agreement in terms of the locations and features with those described above through the OCTS observations. The possible mechanism for this newly identified Chl-a patch is discussed. © 2002 Elsevier Science Inc. All rights reserved.

Keywords: Phytoplankton bloom; Chlorophyll; OCTS; SeaWiFS; Cold SST eddy; Arabian Sea

1. Introduction

In the ocean, the physical, chemical, and biological processes are linked in an intimate manner; the biological and chemical fluxes are, to a certain extent, under physical forcing like wind, currents, mixed layer depth, and temperature (Chaturvedi, Narain, & Pandey, 1998). The northern Arabian Sea is a semienclosed sea (Fig. 1), which experiences seasonal reversal of the surface circulation due to the semiannual monsoon forcing. Despite the observations made in 1990 by the International Indian Ocean Expedition (IIOE) and in 1994–1995 by the Joint Global Ocean Flux Study (JGOFS), larger regions of the northern Arabian Sea, including the Persian Gulf and Gulf of Oman, have remained unknown or poorly known (Martolacci & Luther, 1999; Sarupria & Bhargava, 1998). Recent advances in remote sensing technology allow measure-

ments of phytoplankton/chlorophyll *a* (Chl-a hereafter) concentrations from space (e.g., Sathyendranath et al., 1991; Yoder, McClain, Feldman, & Esaias, 1993). When analyzing ocean color images from the Ocean Color and Temperature Scanner (OCTS) in the Asian waters, we noticed intensive high Chl-a concentrations in the Gulf of Oman in the northwestern Arabian Sea in November 1996. This paper reports on the phytoplankton blooms by time series of Chl-a and SST images and discusses possible blooming mechanisms.

The northern Arabian Sea is one of the most biologically productive ocean regions (Madhupratap et al., 1996). Dynamics and thermodynamics of the surface layer of the Arabian Sea are dominated by the monsoon-related annual cycle of air–sea momentum and heat fluxes. The surface currents in the open-sea region of this layer can be largely accounted for by Ekman drift, and the thermal field is formed by local heat fluxes (Shetye, Gouveia, & Shenoi, 1994). The northern Arabian Sea is renowned for complicated flow pattern consisting of several eddies (Böhm, Morrison, Manghnani, Kim, & Flagg, 1999); little is know

---
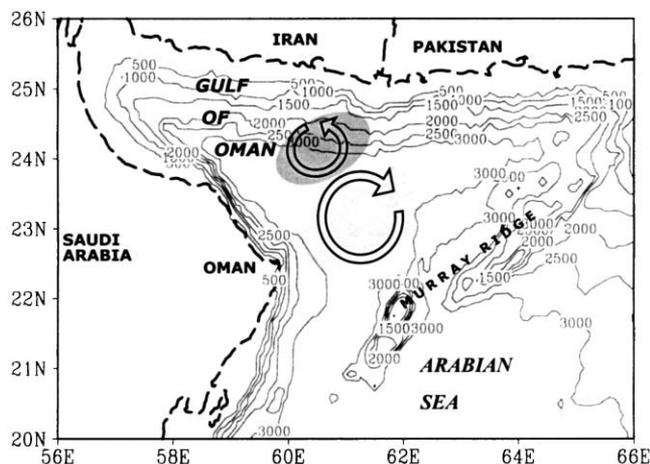
Fig. 1. Geographic location and bathymetry of the study area. The high (low) Chl-a region is patched dark (light) and the circulation pattern is indicated by arrows.

at present about the bottom water circulation in the Arabian Sea (Shetye et al., 1994). Water mass structure in the Arabian Sea is complex (Morrison et al., 1998).

Chl-a concentration, an index of phytoplankton biomass, is the most important property of the marine ecosystem. Remote sensing images of ocean color, converted into Chl-a concentration, provide a window into the ocean ecosystem with synoptic scales. It is a promising approach for understanding the oceanic biological and physical processes, and for the monitoring of ocean waters (Kawamura et al., 1998; Tang, Ni, Kester, & Müller-Karger, 1999; Tang, Ni, Müller-Karger, & Liu, 1998; Yoder et al., 1993). The OCTS sensor aboard the Advanced Earth-Observing Satellite (ADEOS) is one of the new ocean color sensors that was developed after a 10-year hiatus in ocean color records, following the termination of the CZCS observation in 1986. It observed ocean color of global oceans with a high spatial resolution of 700 m from October 1996 to June 1997, and provided voluminous and valuable ocean color data set for oceanographic research (Kawamura et al., 1998). Satellite data can serve as a tool for monitoring the spatial distribution of regional upwelling, the larger-scale ocean patterns, as well as phytoplankton. High-resolution (1 km) Advanced Very High Resolution Radiometer (AVHRR) sea surface temperature (SST) images provide an overall view of upwelling patterns, and ocean color images give Chl-a distributions that may be related to upwelling regions (Ishizaka, Fukushima, Kishino, Saino, & Takahashi, 1992).

While processing the OCTS images for the Asian waters, we noticed prominent features of high Chl-a concentrations in the Gulf of Oman in the northwestern Arabian Sea. In this study, we analyze short-term variation of phytoplankton blooms by using OCTS images, AVHRR SST maps, Sea-view Wide Field-of-view Sensor (Sea-WiFS) images, and other oceanographical data, and address the interrelation between the blooms and the cold

SST eddy with discussions on the possible mechanism for their evolution.

2. Study area, data, and method

2.1. Study area

The bathymetry and the geography of the study area are shown in Fig. 1. In a preliminary screening of OCTS images, patches of high Chl-a concentration were detected in the Gulf of Oman (white circle in Fig. 2). We selected a single study site at the center of the bloom region (60.3–61.3°E, 23.5–24.5°N, indicated by a box on Fig. 3c) for sampling of Chl-a, SST, and the surface parameters.

2.2. Chl-a data

Maps of Chl-a concentrations were derived by using OCTS aboard the ADEOS-1. OCTS images used in this study were processed through SEADAS (Baith, Lindsay, Fu, & McClain, 2001) (MSL 1), adopting the in-water algorithm developed by Kishino, Ishimaru, Furuya, Oishi, and Kawasaki (1998) as part of the ongoing Asian I-Lac Project (Tang & Kawamura, 2001). We processed all available and cloud-free scenes of OCTS to analyze a short-term time series (total 25) for the blooms during November–December 1996. The first available OCTS image was taken on November 2. SeaWiFS data were received by the National Space Development Agency of Japan (NASDA). SeaWiFS images of 1 km spatial resolution were processed through SEADAS at Asian I-Lac Project (Tang & Kawamura, 2001) in Tohoku University, Japan.

2.3. SST data

SST images, corresponding to the OCTS images, are produced from the AVHRR measurement. We use the path-
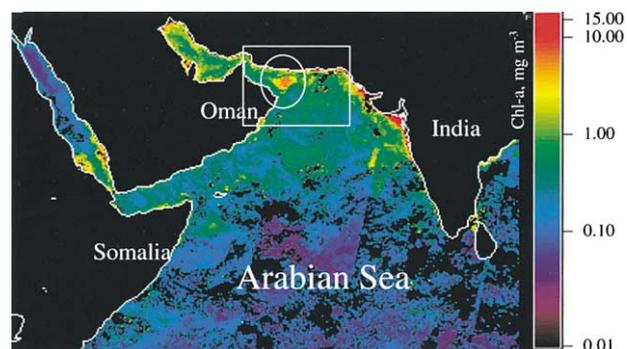
Fig. 2. A composite OCTS image for November 1996 in the Arabian Sea. The land is shown in white color and clouds are in black color. Color bar indicates Chl-a concentrations. High Chl-a concentrations patch (in a white circle) is observed in Gulf of Oman. The box marks the sampling area for OCTS series images.
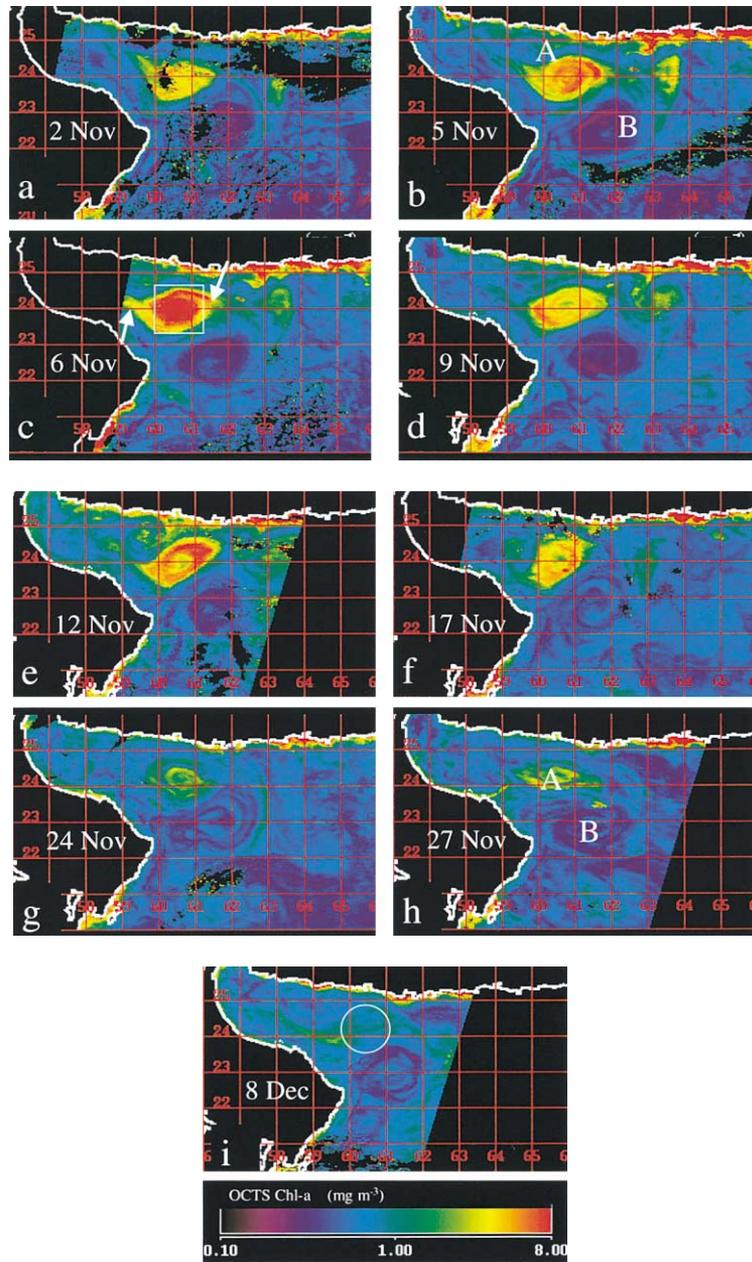
Fig. 3. (a–i) OCTS-derived Chl-a images for the period from November 2 to December 8, 1996. The land is shown in white color and clouds are in black color. Color bar indicates Chl-a concentrations. The box in (c) features the sampling area for Chl-a concentration; the white circle in (i) indicates location of the vanished bloom.

finder (Kilpatrick, Podestá, & Evans, 2001), best-pixel AVHRR SST with spatial resolution of 9 km processed through the Multichannel (MCSST) algorithm, version 4. Coefficients of the MCSST algorithm were calculated over a 5-month period and centered over each month by a least square fit to SST buoys (Vazquez, Perry, & Kilpatrick, 1998). We constructed daily mean SST maps and the gaps between swaths and cloud-masked grids were filled in by 7-day averages. Global statistical measure of the MCSST data relative to drifting buoys shows consistent biases (buoy minus satellite) and root mean square error of $-0.1\ ^{\circ}C$ and $0.5-0.7\ ^{\circ}C$, respectively (McClain, Pichel, & Walton, 1985).

2.4. Other oceanographic data

Surface wind conditions were observed by NASA's scatterometer (NSCAT). Both OCTS and NSCAT were on board the ADEOS-1. To describe the air–sea interaction in the study area, we used NSCAT wind vectors, AVHRR SST, and surface meteorological data including surface net short-wave and long-wave radiation from the National Centers for Environmental Prediction/National Center for Atmospheric Research (NCEP/NCAR) reanalysis data (Kalnay et al., 1996). NSCAT made near-surface wind observations covering 90% of the ice-free ocean every 2 days during Septem-

ber 1996–June 1997. The daily mean maps of NSCAT wind vectors with a spatial resolution of 50 km for November and December 1996 were prepared using successive correction method from NSCAT Level 2 data using the selected ambiguity technique (Tang & Liu, 1996).

The components of turbulent heat flux were estimated through the TOGA/COARE bulk flux algorithm (Fairall, Bradley, Rogers, Edison, & Young, 1996) by coupling the 10-m NSCAT wind components and AHVRR SST with sea level pressure, $2-m$ air temperature, and surface humidity from NCEP/NCAR reanalysis (Kalnay et al., 1996). Surface net heat flux (hereafter Q_{net}) was computed by subtracting the sum of turbulent heat flux estimates and surface net long-wave radiation from surface net short-wave radiation. In this paper, positive heat flux is directed into the ocean. We also estimated the vertical pumping velocity at the base of the mixed layer using $W=(1/\rho f)\nabla \times \tau$, where $\rho = 1025$ kg m^{-3}; $f=2 \times 7.27 \times 10^{-5} \sin(\phi)$; ϕ is latitude; τ is NSCAT-derived wind stress.

3. Results

3.1. Chl-a distribution in the northwestern Arabian Sea

Fig. 2 shows OCTS-derived Chl-a distribution in the northern Arabian Sea in November 1996. Chl-a concentrations are about $0.5-1$ g m^{-3} in the northern Arabian Sea, which are higher than in the southern Arabian Sea (0.1 g m^{-3}). A characteristic feature of high Chl-a (white circle on Fig. 2) is observed in the Gulf of Oman. It is nearly a round-shaped patch with a diameter of 100 km and its edge is about 100 km apart from both sides of the coast. The high Chl-a patch relating to the phytoplankton bloom was present for about 4 weeks.

Fig. 3a–j shows a time series of OCTS Chl-a images to illustrate the temporal variation of the blooms for November 1996. The high Chl-a patch exists for about 4 weeks. On November 2 (Fig. 3a), Chl-a concentration in the patch is about 3 mg m^{-3}. A few days later (on November 6; Fig. 3b), the bloom is intensified and attains a round shape with a

diameter of about 100 km. Spiral features of the high Chl-a patch (Fig. 3b, d, and g) suggest a cyclonic circulation. Another patch of low Chl-a concentrations with a diameter of 100 km (B in Fig. 1b) is located southwest (61.5°E, 22.5°N). In contrast, this eddy shows spiral features that suggest an anticyclonic circulation.

The bloom reaches its peak on November 6, while the highest Chl-a concentration is 9 mg m^{-3} at the center (Fig. 3c). From November 9 to 12 (Fig. 3d and e), the highest Chl-a concentration of 7 mg m^{-3} in the bloom appears in a ring-shaped pattern, and the lower Chl-a values appear at the center. The bloom starts to decay gradually on November 17 (Fig. 3f), loses its round shape on November 24 and 27 (Fig. 3g and h), and disappears on December 8 (Fig. 3i). On the other hand, the patch of lower Chl-a still keeps its characteristic features even in the ending period of the blooming patch.

Fig. 4 shows the distribution of Chl-a concentrations in the northern Arabian Sea obtained from SeaWiFS on November 6, 1998 (Fig. 4a) and on November 7, 1999 (Fig. 4b). There is a pair of circular patches with high and low Chl-a concentrations in the Gulf of Oman. The patch of high Chl-a indicates a cyclonic circulation and the patch of low Chl-a suggests an anticyclonic circulation. These patches are in good agreement, in terms of their locations and features, with those described above through OCTS observations for 1996.

3.2. SST distribution and oceanography data in November–December 1996

The cloud-free SST images for the Gulf of Oman in November 1996 are shown in Fig. 5. To examine the variability in surface conditions, a temporal match of surface Chl-a concentrations (OCTS), AVHRR SST, wind stress, and other water conditions on the bloom area (box in Fig. 3c) is shown in Fig. 6 for the period November 3–December 13, 1996.

The SST on November 6 (Fig. 5a) can be compared with the Chl-a image on November 6 (Fig. 3c). SST is higher in the Gulf of Oman (C in Fig. 5a) than at the outside where the high and low Chl-a patches are seen in the OCTS images
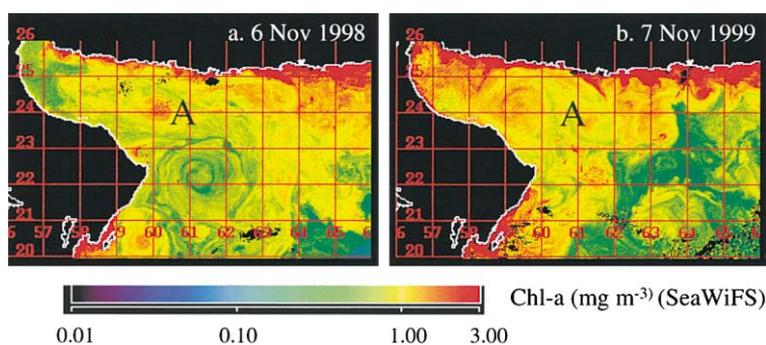
Fig. 4. SeaWiFS-derived Chl-a images on November 6, 1998 (a) and on November 7, 1999 (b). The lands are shown in white color and clouds are in black color. Color bar indicates Chl-a concentrations. (A) indicates a phytoplankton booms area.
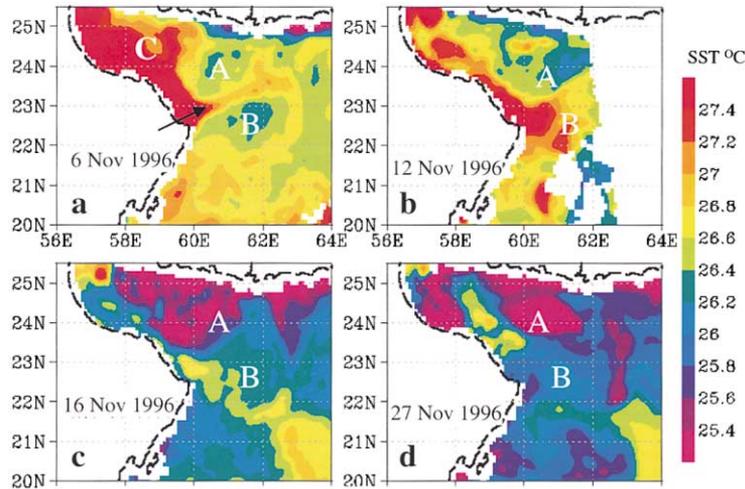
Fig. 5. AVHRR SST images of 9 km spatial resolution showing eddies during November 1996. The bloom with eddy area is 60.3–61.3°E, 23.5–24.5°N (A in Fig. 4), while the anticyclone eddy area is 61.5°E, 22.5°N (B).

(A and B in Fig. 5a), and is an SST front along 60°E. The warm SST region extends outside along the coast of

Fig. 6. Spatial mean time series oceanography data and Chl-a concentrations taken on the box bounded by 23.5–24.5°N and 60.3–61.3°E during November–December 1996. (a) OCTS-derived Chl-a concentrations. A peak appears on November 6 and starts to decrease from November 18 onwards. (b) SST. SST falls by 2 °C during November. There is a peak on November 5. (c) Wind stress. Wind stress exhibits a high peak on November 18. (d) Vertical velocity. There is a peak of the vertical pumping velocity on November 14. (e) Net heat flux.

Oman. The high SST streamer (arrow in Fig. 5a) is elongated from the tip of the warm SST region in between the two characteristic Chl-a patches. This advection of warm water may be attributed to expected circulations, which cause a jet flow towards offshore between them.

On November 12, though SST in the area around the high Chl-a patch (Fig. 3e) decreases, the area around the low Chl-a patch is covered by the warm SSTs extending from the sea along the Oman coast (Fig. 5b). As shown in Figs. 5 and 6b, SSTs decrease gradually from November 6 to 16, which can be attributed to the mechanical mixing due to the wind stress (Fig. 6c) around November 4 and 11 and the outgoing heat flux (Fig. 6e) around November 14. However, the SST decreasing rate during 12–16 is larger in the blooming patch regions (Fig. 5). An SST drop occurred around November 14 (Fig. 6b), which coincides with a peak of the vertical pumping velocity (Fig. 6d). After a small increase of SST after the event on 14th, the strongest peak of wind stress accompanied by the large heat flux (Fig. 6e) and the vertical pumping velocity (Fig. 6d) appear around the 18th. Then, SST decreases largely without recovery for a week. It is suggested that, as well as the heat fluxes, the wind stress inputs vorticity to the blooming area to cause the upwelling of cold subsurface water and intensify the circulation for maintenance of the cyclonic circulation.

4. Discussion

4.1. Phytoplankton bloom in the Gulf of Oman

In the northern Arabian Sea, the surface phytoplankton production ranges from 0.2 to 280.7 mg C m^{-3} day^{-1}; productivity is high in the regions off Bombay, Kutch, and Saurashtra, along Pakistan, and also along southern part of the Gulf of Oman and Yemen (Qasim, 1982). A general

increase in biological productivity was evident in winter (Madhupratap et al., 1996). Field data showed that in the northern Arabian Sea, most of the primary productions occur below the surface during the SW monsoon from June to September; during the NE monsoon (from October to January), the average of the primary production is higher than during the premonsoon from February to May (Qasim, 1982). The highest productivity (100 mg C m^{-3} day^{-1}) region was off the Gulf of Oman. Our OCTS images also show high Chl-a concentrations in the north Arabian Sea in November 1996. This highly productivity during the northern winter is owed to mixing that occurs in the mixed layer due to cooling (Banse, 1987; Madhupratap et al., 1996).

Our OCTS data also show a large phytoplankton bloom with extensively high Chl-a concentrations in an eddy-like feature in the Gulf of Oman. The high Chl-a path was present for 4 weeks in November 1996. Our SeaWiFS images obtained on November 6, 1998 and November 7, 1999 confirm this observation. This bloom has not been documented before. Possible reason may be: (1) the bloom is not year-lived; (2) it is in the middle of Gulf of Oman, far (about 100 km) from coasts; therefore, it could not be easily detected by ship survey. Major questions concerning those phytoplankton blooms are: What is the mechanism for this bloom? What is the interaction between the blooms and the cold SST eddy?

4.2. Possible mechanism of the long-lived blooming in November–December 1996

As presented Section in 4.1, the satellite Chl-a and SST images demonstrated the blooming events occurring between November and December 1996. These satellite evidences can be taken into account to propose a possible mechanism of the biological phenomena related to the eddies and air–sea interaction. Since AVHRR SSTs were uniform before November, there is no satellite evidence of Chl-a and SST for the two eddies in the Gulf of Oman. However, taking the overall situation into consideration, we propose the following as a possible mechanism for the blooming events associated with the eddies, which we hypothesize to preexist in the Gulf of Oman. Formation mechanism of these eddies is unknown at present, and needs to be further investigated, which is however beyond the scope of present study.

(1) There was a pair of cyclonic and anticyclonic eddies around the locations where the first patches appeared in Fig. 3a.

(2) The strong monsoon wind blew from the end of October to November 3 (Fig. 6c), causing mechanical mixing in the surface layer and lifting of the subsurface nutrient to the region of cyclonic eddy, which led to the peak of Chl-a concentration around November 6 (Fig. 6a). However, SST in the Gulf of Oman did not decrease (Fig. 6b) in the beginning of November because of absence of heat loss (Fig. 6e) and upward pumping velocity (Fig. 6d).

(3) The wind stress curl relating to the vertical pumping velocity was imposed on the cyclonic eddy at around November 14. It caused an SST decrease again in the blooming region and supplied additional nutrients to the surface layer, which intensified the cyclonic circulation and maintained the succeeding phytoplankton blooming towards December. The same mechanism occurred at around November 18.

On November 12, though SST in the area around the high Chl-a patch (Fig. 3e) decreases, the area around the low Chl-a patch is covered by the warm SSTs extending from the sea along the Oman coast (Fig. 5b). As shown in Figs. 5 and 6b, SSTs decrease gradually from November 6 to 16, which can be attributed to the mechanical mixing due to the wind stress (Fig. 6c) around November 4 and 11 and the outgoing heat flux (Fig. 6e) around November 14. However, the SST decreasing rate during 12–16 is larger in the blooming patch regions (Fig. 5). An SST drop occurred around November 14 (Fig. 6b), which coincides with a peak of the vertical pumping velocity (Fig. 6d). After a small increase of SST following the event noticed on November 14, the strongest peak of wind stress, accompanied by the large heat flux (Fig. 6e) and the vertical pumping velocity (Fig. 6d), appears around November 18. Then, SST decreases largely without recovery for a week. Wind directions on November 11, 14, and 18 are all from the north, i.e., the northerly winds. Eastern component is also slightly included. It is suggested that, like the heat fluxes, the wind stress inputs vorticity to the blooming area, which causes the upwelling of cold subsurface water and intensifies the circulation for maintenance of the cyclonic circulation

In the northern Arabian Sea, the rate of phytoplankton cell division is controlled by nutrient availability rather than light, while light inhibition of photosynthesis near the surface is negligible (Banse, 1987, 1994). There is little river discharge (cf. 208 km^3 year^{-1}) in the northern Arabian Sea, and most of the nutrients (phosphate) appear to come from subsurface layers by thermocline convection (Qasim, 1982). Our results show that the Chl-a blooms coincide with the cold SST eddy, which is in agreement with the fact that the blooms are promoted by local upwelling. The cold and warm water masses correspond to a northern cyclonic eddy and a southern anticyclonic eddy, respectively, which is in agreement with that described in a previous study as a large meander demarcates two counter-rotation eddies (Böhm et al., 1999).

The circulation in the coastal region off Oman is driven mainly by local winds and there is no remotely driven western boundary current of this area. During the northeast monsoon (November–February), the winds blow from the northeast and have maximum wind stress magnitudes of about 2 dyn cm^{-2} (Shetye et al., 1994). The circulation pattern consists of several eddies and meanders, with a pronounced anticyclonic eddy around 24°N, 64°E. In general, eddies appear to have appreciable deep vertical extension (Qasim, 1982). The eddy circulation is attributed to

the influence of bottom topography, which is marked by depressions and rises (Das, Gouveia, & Varma, 1980).

5. Conclusion

Using high-resolution OCTS images, AVHRR SST maps, SeaWiFS images, and inferences from surface atmospheric heat budget, we observed the short-term variability of phytoplankton blooms that appeared in the Gulf of Oman over a 4-week period in November 1996. There was a pair of a cyclonic and an anticyclone eddies around the locations of blooming event. The Chl-a images provided a continuous monitoring of the bloom, while the AVHRR SST indicated that the bloom is associated with a cold SST eddy. The pair of cyclonic and anticyclones eddies can be considered to be influenced by the wind stress associated with the winter monsoon.

This is the first observation of phytoplankton blooms coinciding with a cold SST eddy, featuring its short-term variability in the Gulf of Oman by satellite images. This study further demonstrates the potential of using satellite ocean color and SST images to monitor short-term variability of phytoplankton distributions, and to detect the interaction between phytoplankton blooms and other dynamical oceanic features.

Acknowledgments

References

Baith, K., Lindsay, R., Fu, G., & McClain, C. R. (2001). SeaDAS: data analysis system developed for ocean color satellite sensors. *Eos*, *82* (18), 202.

Banse, K. (1987). Seasonality of phytoplankton chlorophyll-*a* in the central and northern Arabian Sea. *Deep-Sea Research*, *34*, 713–723.

Banse, K. (1994). On the coupling of hydrography, phytoplankton, zooplankton, and settling organic particles offshore in the Arabian Sea.

Proceeding of the Indian Academy of Science (Earth Planet Science), *103*, 99–106.

Böhm, E., Morrison, J. M., Manghnani, V., Kim, H.-S., & Flagg, C. N. (1999). The Ras al Hadd Jet: remotely sensed and acoustic Doppler current profiler observations in 1994–1995. *Deep–See Research, Part II*, *46*, 1531–1548.

Chaturvedi, N., Narain, A., & Pandey, P. C. (1998). Phytoplankton pigment/temperature relationship in the Arabian Sea. *Indian Journal of Marine Sciences*, *27*, 286–291.

Das, V. K., Gouveia, A. D., & Varma, K. K. (1980). Circulation and water characteristics on isanosteric surfaces in the northern Arabian Sea. *Indian Journal of Marine Sciences*, *9*, 156–165.

Fairall, C. W., Bradley, E. F., Rogers, D. P., Edison, J. B., & Young, G. S. (1996). Bulk parameterization of the air–sea fluxes for Tropical Ocean-Global Atmosphere-Coupled Ocean Response Experiment. *Journal of Geophysical Research*, *101*, 3747–3764.

Ishizaka, J., Fukushima, H., Kishino, M., Saino, T., & Takahashi, M. (1992). Phytoplankton pigment distributions in regional upwelling around the Izu Peninsula detected by coastal zone color scanner on May 1982. *Journal of Oceanography*, *48*, 305–327.

Kalnay, E., Kanamitsu, M., Kistler, R., Collins, W., Deaven, D., Gandin, L., Iredell, M., Saha, S., White, G., Woollen, J., Zhu, Y., Chelliah, M., Ebisuzaki, W., Higgins, W., Janowiak, J., Mo, K. C., Ropelwski, C., Wang, J., Leetmaa, A., Reynolds, R., Jenne, R., & Joseph, D. (1996). The NCEP/NCAR 40-year reanalysis project. *Bulletin of American Meteorological Society*, *77*, 437–471.

Kawamura, H. & OCTS Team (1998). OCTS mission overview. *Journal of Oceanography*, *54*, 383–399.

Kilpatrick, K. A., Podestá, G. P., & Evans, R. (2001). Overview of the NOAA/NASA Advanced Very High Resolution Radiometer pathfinder algorithm for sea surface temperature and associated mathcup database. *Journal of Geophysical Research*, *106* (C5), 9179–9197.

Kishino, M., Ishimaru, T., Furuya, K., Oishi, T., & Kawasaki, K. (1998). In-water algorithms for ADEOS/OCTS. *Journal of Oceanography*, *54* (5), 431–436.

Madhupratap, M., Kumar, S. P., Bhattathiri, P. M. A., Raghukumar, S., Nair, K. K. C., & Ramaiah, N. (1996). Mechanism of the biological response to winter cooling in the northeastern Arabian Sea. *Letters to Nature*, *384*, 549–552.

Martolacci, D. M., & Luther, M. E. (1999). Patterns of co-variability between physical and biological parameters in the Arabian Sea. *Deep-Sea Research, Part II*, *46*, 1933–1964.

McClain, E. P., Pichel, W. G., & Walton, C. C. (1985). Comparative performance of AVHRR based multichannel sea surface temperatures. *Journal Geophysical Research*, *90*, 11587–11601.

Morrison, J. H., Codispoti, L. A., Gaurin, S., Jones, B., Manghnani, V., & Zheng, Z. (1998). Seasonal variation of hydrographic and nutrient fields during the US JGOFS Arabian Sea Process Study. *Deep-Sea Research, Part II*, *45*, 2053–2101.

Qasim, S. Z. (1982). Oceanography of the northern Arabian Sea. *Deep-Sea Research*, *29* (9a), 1041–1068.

Sarupria, J. S., & Bhargava, R. M. S. (1998). Seasonal distribution of chlorophyll-*a* in the Exclusive Economic Zone (EEZ) of India. *Indian Journal of Marine Sciences*, *27*, 292–297.

Sathyendranath, S., Platt, T., Horne, E. P. W., Harrison, W. G., Ulloa, O., Outerbridge, R., & Hoepffner, N. (1991). Estimation of new production in the ocean by compound remote sensing. *Nature*, *353*, 129–133.

Shetye, S. R., Gouveia, A. D., & Shenoi, S. S. C. (1994). Circulation and water masses of the Arabian Sea. In: D. Lal (Ed.), *Biogeochemistry of the Arabian Sea* (pp. 9–25). New Delhi: Indian Academy of Sciences (Phototypeset at Thomson Press, India).

Tang, D. L., & Kawamura, H. (2001). Long-term time series satellite ocean color products on the Asian waters. In: *Proceedings of the 11th PAMS/JECSS workshop* (pp. 49–52). Seoul, South Korea: Hanrimwon Publishing (CD-ROM: O112-P-03).

Tang, D. L., Ni, I-H., Kester, D. R., & Müller-Karger, F. E. (1999). Remote sensing observation of winter phytoplankton blooms southwest of the

Luzon Strait in the South China Sea. *Marine Ecology Progress Series*, *191*, 43–51.

Tang, D. L., Ni, I-H., Müller-Karger, F. E., & Liu, Z. J. (1998). Analysis of annual and spatial patterns of CZCS-derived pigment concentrations on the continental shelf of China. *Continental Shelf Research*, *18*, 1493–1515.

Tang, W., & Liu, W. T. (1996). Objective interpolation of scatterometer winds. *Jet Propulsion Laboratory Publication*, *96–19*, 1–16.

Vazquez, J., Perry, K., & Kilpatrick, K. (1998). NOAA/NASA AVHRR oceans pathfinder sea surface temperature data set. User's reference manual, version 4.0. *Jet Propulsion Laboratory Publication*, 74 (D-14070).

Yoder, J. A., McClain, C. R., Feldman, G. F., & Esaias, W. E. (1993). Annual cycles of phytoplankton chlorophyll-*a* concentrations in the global ocean: a satellite view. *Global Biogeochemcal Cycles*, *7*, 181–193.